NUEJ
Naresuan University
Engineering Journal

Study of Unbalanced Voltage on Rotor Classes of Induction Motor According to NEMA Standard

K. Kraikitrat[1], S. Ruangsinchaiwanich[2], and D. Phaengkieo[3*]

[1] Department of Electrical Engineering, Faculty of Engineering, University of Phayao, Phayao, Thailand
[2] Department of Electrical and Computer Engineering, Faculty of Engineering, Naresuan University, Phitsanuloke, Thailand
[3] Department of Electrical Engineering, Faculty of Engineering, Rajamangala University of Technology Lanna Phitsanulok, Phitsanulok, Thailand

[*]Corresponding author e-mail: duanraem@rmutl.ac.th

(Received: 2 May 2023, Revised: 21 November 2023, Accepted: 1 December 2023)

Abstract

This investigation studies core loss and thermal distributions. There are four types of 3-phase induction motors that meet the National Electrical Manufacturers Association (NEMA) standard when receiving unbalanced voltage by testing the motor under unbalanced voltage conditions. The conditions are different. The model analysis method was used in conjunction with the Finite Element Method (FEM) as well as experimental and computational theory. To analyze the change in magnetic flux density and the resulting temperature. Along with finding a conclusion on the effect on the motor when the voltage is unbalanced.

Keywords: FEM, Flux Distributions **,** Induction Motor, Thermal distributions, Unbalanced Voltage Conditions.

1. INTRODUCTION

Electricity is a crucial element for economic growth and national security. When the power system is abnormal, such as when the magnitudes of phase or line voltages are distinct, and the phase angles differ from balanced conditions or both, Etc., it is detrimental to the system's overall performance because even the smallest imbalance will have a significant effect on the electrical equipment particularly 3-phase induction motors, which are extensively utilizing. The operating parameters vary if the motor operates under an unbalanced voltage condition. Consequently, the motor's performance is altering and may be damaged. The National Electrical Manufacturers Association (NEMA) has classified the various types of induction motors so that the appropriate selection can be made based on the nature of the activity. Each variety is characterized by its Torque-Speed. However, NEMA has not clarified how Core Loss and Thermal differ between motor types. Therefore, this study investigated the effect of Core Loss. Furthermore, Thermal occurs in each motor type under unbalanced input voltage conditions.

Faults of the electrical system, for example, unbalanced voltage conditions and inconsistent frequency, is frequently occurred, which reduces the quality of the electrical system and affects the efficiency of electrical appliances, especially electrical motors (Kersting & Phillips, 1997; Ching-Yin Lee et al., 1997; Siddique et al., 2004; Chen, K., 2009).

This paper analyzes the effects of unbalanced voltage conditions on the Core Loss and Thermal Analysis of Class A, B, C, and D motors according to NEMA standards by specifying and designing all four motor models with identical rotor volumes. Twenty cases are computed using the Line voltage unbalance rate (LVUR) and Phase voltage unbalance rate (PVUR) methods to ascertain the voltage unbalance condition.

2. UNBALANCE VOLTAGE CONDITIONS

Various standards have provided the following three definitions of voltage imbalances. The National Electrical Manufacturers Association (NEMA) standard MG1-1993 defines voltage unbalance, also known as the line voltage unbalance rate (LVUR).

$$\%\ \text{LVUR} = \frac{\text{Max voltage deviation-from the avg line voltage}}{\text{avg line voltage}} \times 100\% \quad (1)$$

The IEEE defines voltage unbalance, called the phase voltage to unbalance rate (PVUR).

$$\%\ \text{PVUR} = \frac{\text{Max voltage deviation-from the avg phase voltage}}{\text{avg phase voltage}} \times 100\% \quad (2)$$

Genuine Definition: The ratio of the negative sequence voltage component to the positive sequence voltage component is the simple definition of voltage unbalance (R.C. Dugan et al., 1996). The true definition of the percentage voltage disequilibrium factor (% VUF) is given by

$$\% \text{ VUF} = \frac{\text{Negative sequence-voltage component}}{\text{Positive sequence-voltage component}} \times 100\% \quad (3)$$

3. Induction Motor of NEMA Designs Class

The national electrical manufacturers association (NEMA) defines a series of standard rotor-shape designs with different torque-speed characteristics. Figure 1 shows the prototype of a class B rotor induction motor, the main motor components, and the mesh of the 3D FEM model.

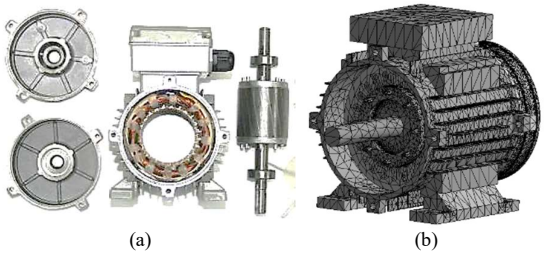

(a) (b)

Figure 1 Prototype of class B induction motor
(a) main motor components, (b) mesh of 3D FEM model

3.1 Stator Dimensions

Figure 2 depicts the dimensions of the induction motor prototype and the diameters of the stator and rotor.

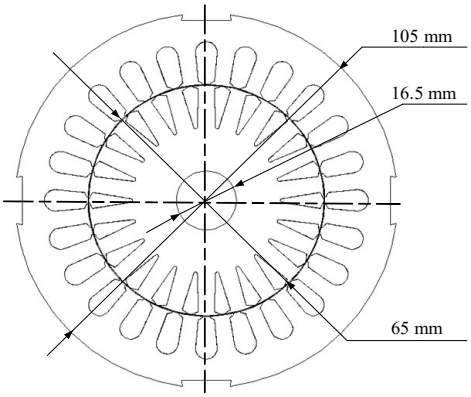

Figure 2 Dimension of the prototype induction

3.2 Rotor Dimensions of NEMA Designs

(a) (b) (c) (d)

Figure 3 Dimension of rotors
(a) class A (b) class B (c) class C (d) class D

The NEMA specification guides the design of the rotors utilized in this investigation. To facilitate comparison, the volume of each of the four rotor classes is identical. The prototype of rotor configurations, including classes A, B, C, and D, is illustrated in Figure 3.

4. Analysis Of Result

Several methods can illustrate the effect of unbalanced voltage conditions on an induction motor. In this paper, FEM calculation is focused on. FEM is largely accepted as a significant method for analyzing the electromagnetic field, particularly electrical machines' performances.

The impact of rotor bar slot geometry on core loss and heat transfer is analyzed. In this study, the rotor volumes of all four varieties are equivalent. Before analyzing these effects on the prototype motor and models of all four categories of motors, these effects must be analyzed on the prototype motor. In the example depicted in Figures 4 and 5, the situation is as shown.

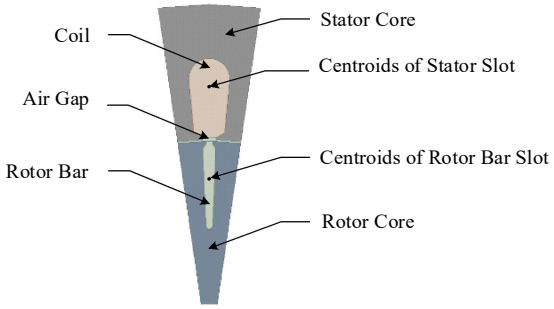

Figure 4 Dimension of sample model

Despite sharing an identical capacity, the four variants of motors differ in the configuration of the slots on the rotor bar. As illustrated in Figure 5, this investigation is also capable of identifying discrepancies in rotor bar slot geometries, specifically the distance between the rotor bar slot's centroid and the stator slot. The thermal and core loss are directly influenced by the centroid of the rotor opening.

(a) (b) (C) (d)

Figure 5 Examples of motor models (a) class A (b) class B (c) class C (d) class D

4.1 Flux distributions

Magnetic field density can be derived from Equation (4), that is, by calculating the magnetic flux (ϕ) per unit area (A) that travels through the conductor.

$$B = \frac{\phi}{A} \tag{4}$$

When contemplating the transient for a 3D Cartesian problem, the magnetic field's mathematical model can be expressed as a second-order partial differential equation.

$$\frac{\partial}{\partial x}\left(\frac{1}{\mu}\frac{\partial A}{\partial x}\right)+\frac{\partial}{\partial y}\left(\frac{1}{\mu}\frac{\partial A}{\partial y}\right)+\frac{\partial}{\partial z}\left(\frac{1}{\mu}\frac{\partial A}{\partial z}\right)=-J+\sigma\frac{\partial A}{\partial t} \tag{5}$$

Where (A) is the desired magnetic vector potential, μ is the magnetic permeability, σ is the electrical conductivity, ω is the angular velocity, and J is the current density at is obtained from an external power source, and i is the imaginary part. The term $\sigma(\partial A/\partial t)$ represents the current induced in the conductor material as the magnetic flux changes with time.

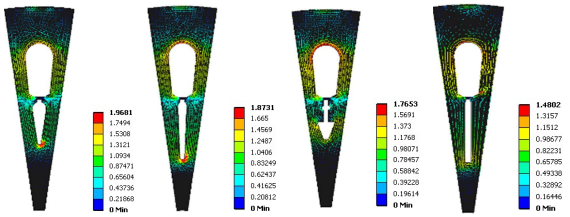

(a) (b) (c) (d)

Figure 6 Flux distributions of motor model examples by FEM (a) class A (b) class B (c) class C (d) class D

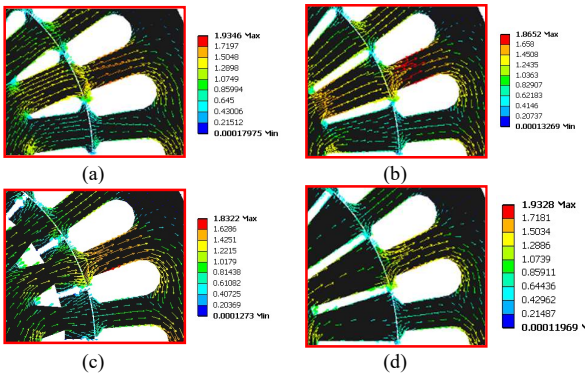

(a) (b) (c) (d)

Figure 7 Flux distributions of motors by FEM (a) class A (b) class B (c) class C (d) class D

The induced magnetic flux on the iron centers of the stator and rotor is illustrated in Figures 6 and 7. Using the FEM method, the no-load voltage rating is calculated from the example model in Figure 5 and the normal-sized motor model. As illustrated in Figure 6, the stator and rotor conductor currents produce magnetic flux in the stator and rotor iron cores. As a result, the magnetic flux that the motor produces is equal to the sum of the two magnetic fluxes. The distinct total magnetic fluxes result from the fact that the volume of the rotor bar slots remains constant while the centers of the slots' geometries (centroid points) vary. The magnetic flux in Fig. 6(d) is greater than in Fig. 6(a) due to the shorter distance between the conductor centers that produce the two magnetic flux sources. As a result, the magnetic flux will be amalgamated as well.

As shown in Equations (6) and (7), the magnetic field density immediately affects the iron core losses. Equation (6) illustrates the typical combination of hysteresis and eddy current losses that contribute to the iron core losses in the stator and rotor.

$$P_c = P_h + P_e$$

$$P_c = k_h f B^n + k_e f^2 B^2 \tag{6}$$

Where P_c is Core Loss, P_h is Hysteresis Loss, P_e is Eddy Current loss, k_h, k_e and n is Coefficients, f is Frequency, and B is the Peak value of the Magnetic Flux. Density. However, the effect of increased losses in the case of high frequencies has been added to increase the eddy current. Therefore, the calculation formula becomes.

$$P_c = P_h + P_e + P_a$$

$$P_c = k_h f B^n + k_e f^2 B^2 + k_a f^{1.5} B^{1.5} \tag{7}$$

Where P_a is Excess Loss and k_a is Coefficients.

Table 1 The core loss of induction motor class B

Conditions	Core Loss (W)		Error (%)
	Analysis	FEM	
Balance	31.3101	31.2759	0.1092
Under 1⌀ 1 Percent	30.9989	31.1185	0.3825
Under 1⌀ 2 Percent	30.6915	30.9281	0.7566
Under 1⌀ 3 Percent	30.3972	30.7317	1.0695
Under 1⌀ 4 Percent	30.1064	30.5326	1.3626
Under 1⌀ 5 Percent	29.8281	30.3242	1.5861
Under 2⌀ 1 Percent	30.6881	31.1018	1.3228
Under 2⌀ 2 Percent	30.0932	30.9015	2.5843
Under 2⌀ 3 Percent	29.5245	30.6985	3.7536
Under 2⌀ 4 Percent	28.9633	30.4961	4.9010
Under 2⌀ 5 Percent	28.4274	30.2813	5.9274
Over 1⌀ 1 Percent	31.6251	31.4237	0.6312
Over 1⌀ 2 Percent	31.9537	31.5684	1.2075
Over 1⌀ 3 Percent	32.2863	31.6898	1.8693
Over 1⌀ 4 Percent	32.6230	31.8081	2.5539
Over 1⌀ 5 Percent	32.9638	31.9096	3.3037
Over 2⌀ 1 Percent	31.9405	31.4405	1.5630
Over 2⌀ 2 Percent	32.5990	31.5954	3.1373
Over 2⌀ 3 Percent	33.2863	31.7405	4.8321
Over 2⌀ 4 Percent	34.0033	31.8724	6.6611
Over 2⌀ 5 Percent	34.7304	31.9910	8.5632

Table 1 shows the iron core loss of a prototype Class B motor under mechanical load at various voltage unbalanced conditions between the FEM method and the calculation. Furthermore, Figures 8 and 9 show the effect of voltage unbalance on core loss power, both under normal and above normal pressure conditions, while the motor operates without mechanical load.

Figure 10 depicts the influence of unbalanced voltage conditions on iron core power loss. Under typical and above normal voltage conditions for all four types of motors, While the motor operates without mechanical load, Figure 11 compares the core loss power under equilibrium voltage conditions while driving various mechanical load levels among the four motor varieties.

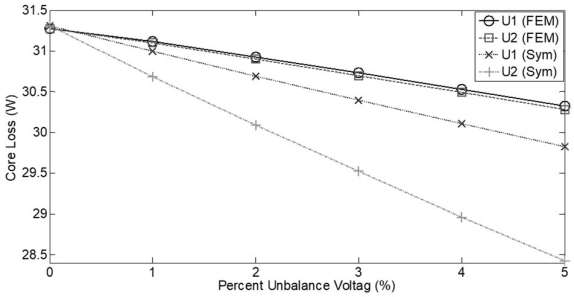

Figure 8 Core loss of the class B motor with under voltage conditions

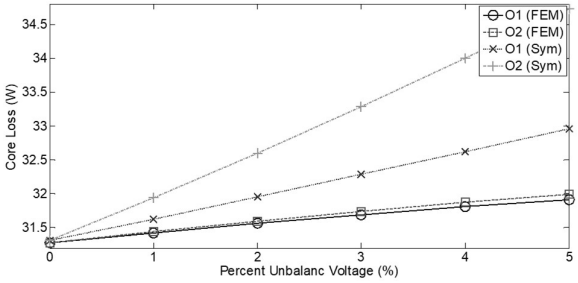

Figure 9 Core loss of the class B motor with over voltage conditions

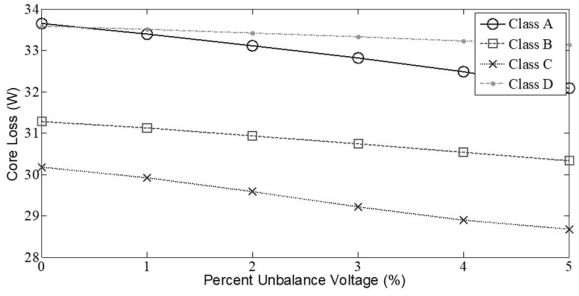

(a)

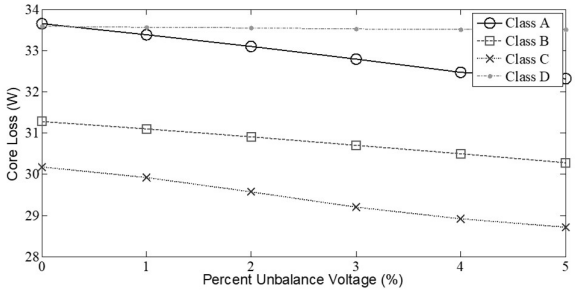

(b)

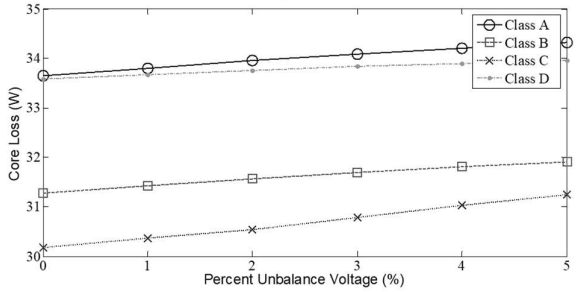

(c)

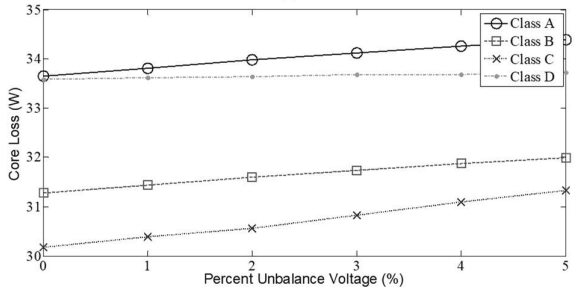

(d)

Figure 10 Core loss of motor class A, B, C and D
(a) under voltage 1 Phase (b) under voltage 2 Phase
(c) over voltage 1 Phase (d) over voltage 2 Phase

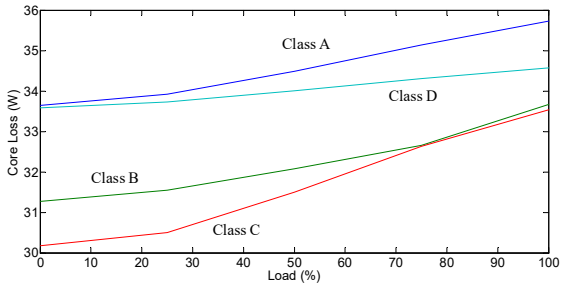

Figure 11 Core loss comparison of motors

4.2 Thermal Distributions

Heat Transfer is the exchange of hot energy. as a result of the temperature difference, and it drives the heat flow from high temperature to low temperature.

$$q = -k.A.\frac{T_2 - T_1}{L} \tag{8}$$

Equation (8) shows the thermal conductivity rate that is directly proportional to the temperature difference at

both sides of the object (T_1 and T_2) and the surface area perpendicular to the heat flow direction (A) and is inversely proportional to the thickness of the object (L).

Figure 12 illustrates two sources of heat in the motor: the stator windings and the rotor bar openings. In Fig. 12(a), the distance between the two sources (centroid point) is smaller than the distance between the sources in Fig. 12(d), resulting in more significant maximal heat generation than in Fig. 12(d).

The 3D-heat conduction equation, which can describe steady-state and transient temperature distribution in the solution region (Ω), is regulated by the differential equation (9):

$$-\left(\frac{\partial q_x}{\partial x}+\frac{\partial q_y}{\partial y}+\frac{\partial q_z}{\partial z}\right)+q_O=\rho c\frac{\partial T}{\partial t} \tag{9}$$

Where q_x, q_y and q_z heat flow rate of x, y, z directions respectively; q_O heat generation; ρ mass density (kg/m^3), c specific heat capacity; T temperature (^oC).

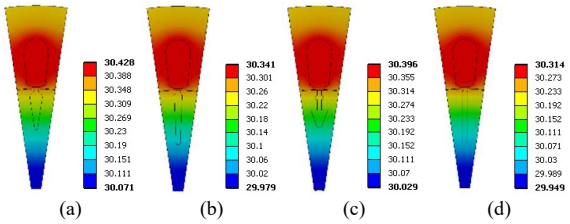

Figure 12 Thermal distributions of motor model examples by FEM (a) class A (b) class B (c) class C (d) class D

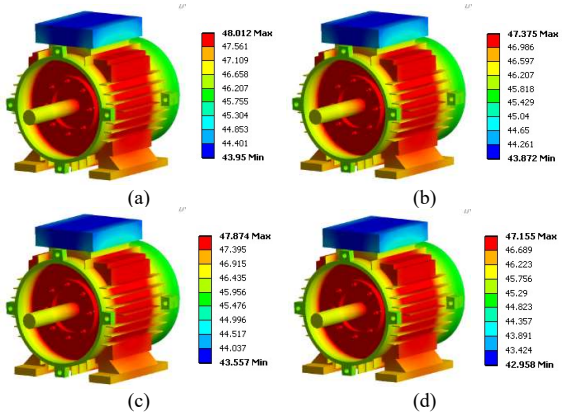

Figure 13 Thermal distributions of motors by FEM (a) class A (b) class B (c) class C (d) class D

Figure 12 is the result of the analysis of how the rotor bar geometry affected the heat that the sample simulation in Figure 5 produced. Additionally, the findings of the investigation into the impact of the rotor bar slot geometry on the heat produced in four different types of conventional motors are presented in Figure 13. It was observed that the heating effect of the rotor bar varied depending on its geometry. As shown in Tables 2 and 3, Figure 14 is a thermal camera image of a prototype Class B motor operating under varying voltage and mechanical load conditions. Additionally, Figures 15 and 16 compare the heat the prototype Class B motor produces experimentally and using FEM. It was observed that both approaches produced thermal energy in the motor in the identical direction.

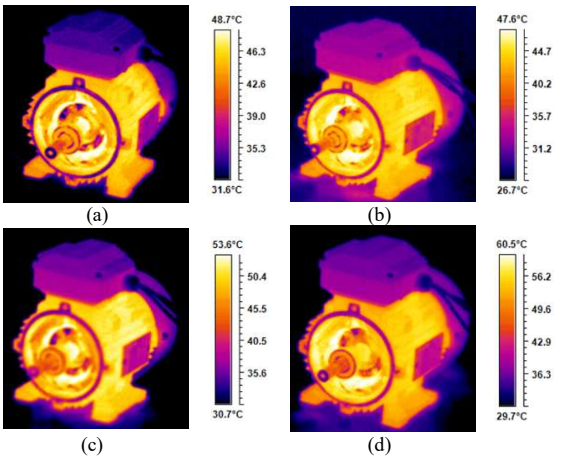

Figure 14 Thermal distribution of the class B motor by measurement with balancing voltage at no load condition

Table 2 Maximum temperature of induction motor class B

Load (%)	Maximum Temperature (°C)		
	Test	FEM	Error
0	47.9	47.375	1.096
25	48.9	49.379	0.979
50	53.1	54.831	3.259
75	61.0	63.388	3.914
100	73.6	74.716	1.516

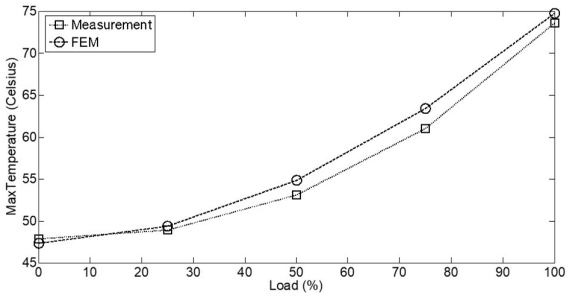

Figure 15 Maximum temperature of motors

Table 3 Maximum temperature of induction motor class B

Conditions	Maximum Temperature (°C)		
	Test	FEM	Error
Balance Voltage	47.9	47.375	1.096
Under Voltage 1 Phase 5%	47.3	46.774	1.112
Under Voltage 2 Phase 5%	44.8	45.617	1.823
Over Voltage 1 Phase 5%	52.2	49.390	5.383
Over Voltage 2 Phase 5%	55.2	50.849	7.882

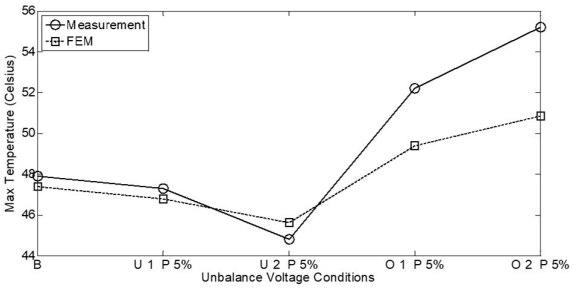

Figure 16 Maximum temperature of motors

When contemplating the effects of unbalanced voltage conditions on the heat generated by the four types of motors, under both normal and overvoltage conditions, while the motor is operating without mechanical load: Figure 17 depicts the result, and Figure 18 compares the heat generated by all four types of motors while driving various levels of load.

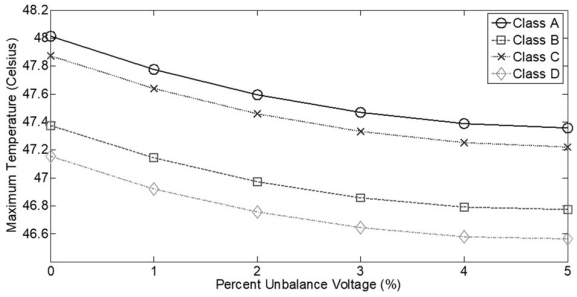

(a)

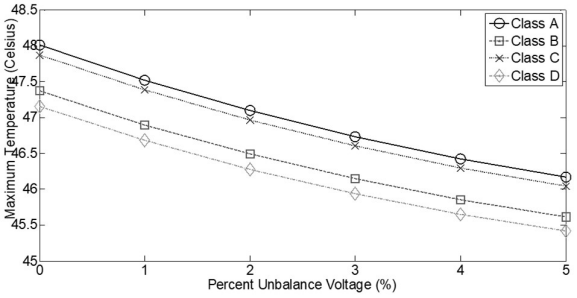

(b)

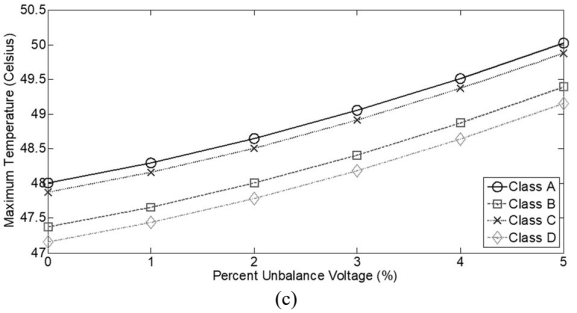

(c)

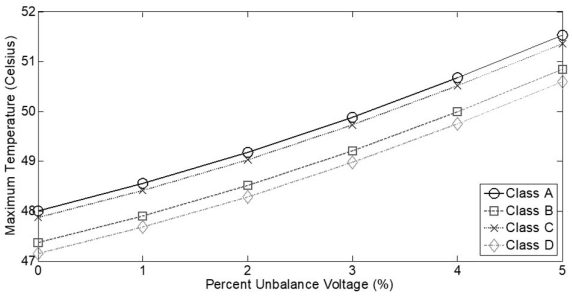

(d)

Figure 17 Maximum temperature of motor class A, B, C and D (a) under voltage 1 Phase (b) under voltage 2 Phase (c) over voltage 1 Phase (d) over voltage 2 Phase

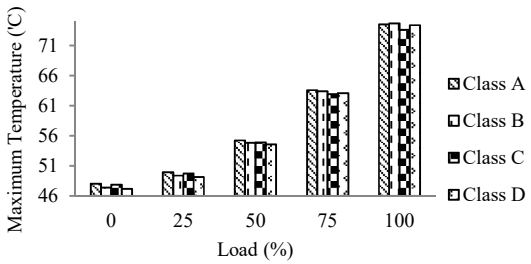

Figure 18 Maximum temperature comparison of motors

5. CONCLUSION

They are considering the effects of unbalanced voltages on iron core loss and heat generation in all four varieties of motors with identical rotor area specifications. The following results: Iron core loss is most significant in Class A motors. Because the distance between the centers of the conductors causes the two sources of magnetic flux to be shorter than in other motors, there is a possibility that the magnetic flux will also be combined. The value of magnetic flux is directly proportional to the resulting iron core loss. Class A motors were discovered to produce the most heat in terms of heat output. Since the distance between the two heat sources is the shortest between the stator winding and the rotor bar, the temperature accumulation is most significant.

Consider the various rotor shapes of the four varieties and the iron core loss and heat generated. Consequently, it can be concluded that, in addition to the size of the rotor bar, the geometry of the rotor bar also plays a role. This affects the iron core depletion and heat produced. The geometry factor may have less impact than the dimension factor. Therefore, when contemplating the selection of a motor, the rotor bar's size must be considered, which is the most critical factor in conjunction with the geometry of the rotor bar.

6. ACKNOWLEDGMENT

The author would like to express his gratitude to the Fundamental Fund Research and Innovation Research Budget Program, Thailand Science Research and Innovation (TSRI) Contract Number FF66-RIM033, and the Faculty of Engineering, University of Phayao for providing a space for research.

7. REFERENCES

Kersting, W. H., & Phillips, W. H. (1997). Phase frame analysis of the effects of voltage unbalance on induction machines. *IEEE Transactions on Industry Applications, 33*(2), 415-420.

Lee, C. Y., Chen, B. K., Lee, W. J., & Hsu, Y. F. (1998). Effects of various unbalanced voltages on the operation performance of an induction motor under the same voltage unbalance factor condition. *Electric Power Systems Research, 47*(3), 153-163.

Siddique, A., Yadava, G. S., & Singh, B. (2004, September). Effects of voltage unbalance on induction motors. *In Conference Record of the 2004 IEEE International Symposium on Electrical Insulation* (pp. 26-29). IEEE.

Chen, K. (2009, March). Iron-loss simulation of laminated steels based on expanded generalized steinmetz equation. *In 2009 Asia-Pacific Power and Energy Engineering Conference* (pp. 1-3). IEEE.

Motors and Generators, *ANSI/NEMA Standard MG1-1993*.

IEEE Standard Test Procedure for Polyphase Induction Motors and Generators, *IEEE Standard 112*, 1991.

Dugan, R. C., McGranaghan, M. F., & Beaty, H. W. (1996). *Electrical power systems quality*. New York.

Hwang, C. C., Tang, P. H., & Jiang, Y. H. (2005). Thermal analysis of high-frequency transformers using finite elements coupled with temperature rise method. *IEE Proceedings-Electric Power Applications, 152*(4), 832-836.

Reece, A. B. J., & Preston, T. W. (2000). *Finite element methods in electrical power engineering (Vol. 46).* Courier Corporation.

Shumei, C., Ying, D., & Liwei, S. (2006, September). Rotor slots design of induction machine for hybrid electric vehicle drives. *In 2006 IEEE Vehicle Power and Propulsion Conference* (pp. 1-3). IEEE.

Kirtley, J. L., Cowie, J. G., Brush, E. F., Peters, D. T., & Kimmich, R. (2007, June). Improving induction motor efficiency with die-cast copper rotor cages. *In 2007 IEEE Power Engineering Society General Meeting* (pp. 1-6). IEEE.

Turcanu, O. A., Tudorache, T., & Fireteanu, V. (2006, May). Influence of squirrel-cage bar cross-section geometry on induction motor performances. In International Symposium on Power Electronics, Electrical Drives, Automation and Motion, 2006. *SPEEDAM 2006*. (pp. 1438-1443). IEEE.

Fireteanu, V., Tudorache, T., & Turcanu, O. A. (2007, May). Optimal design of rotor slot geometry of squirrel-cage type induction motors. *In 2007 IEEE International Electric Machines & Drives Conference* (Vol. 1, pp. 537-542). IEEE.

Pillay, P., & Manyage, M. (2001). Definitions of voltage unbalance. *IEEE Power Engineering Review, 21*(5), 50-51.

8. BIOGRAPHIES

Kreangsuk Kraikitrat
Currently working as an Asst. Prof. at the Department of Electrical Engineering Faculty of Engineering, University of Phayao.

Somporn Ruangsinchaiwanich
Department of Electrical and Computer Engineering, Faculty of Engineering, Naresuan University, Muang, Phitsanuloke, Thailand

Duanraem Phaengkieo
Department of Electrical Engineering, Faculty of Engineering, Rajamangala University of Technology Lanna Phitsanulok, Phitsanulok, Thailand